Deep Eutectic Solvent Membranes Designed by the Same-Anion Strategy for Highly Efficient Ethylene/Ethane Separation

Mi Xu, Haozhen Dou, Yanxiong Ren, Feifei Peng, Xiaoming Xiao, Xiaowei Tantai, Yongli Sun, Bin Jiang, Na Yang,* and Luhong Zhang*

Read Online

ACCESS | Metrics & More | Article Recommendations | Supporting Information

ABSTRACT: Deep eutectic solvents (DESs) are a new generation of designer and green solvents and offer tremendous opportunities for separation science; however, the construction of high-permeance DES membranes (DESMs) with excellent stability for ethylene/ethane separation is still a challenge. In this study, by the same-anion strategy, a series of DESs with the $CF_3SO_3^-$ anion were designed for the first time and then combined with an ethylene transport carrier ($AgCF_3SO_3$) for the construction of DESMs for highly efficient ethylene/ethane separation. DESMs were facilely fabricated by impregnating the as-designed DESs and $AgCF_3SO_3$ carrier into the commercial poly(vinylidene fluoride) membrane, where the DESs not only exhibited good compatibility with $AgCF_3SO_3$ but also stimulated high carrier activity and afforded good carrier stability. The resultant DESMs displayed high ethylene permeability, ethylene/ethane selectivity, and excellent stability, especially the maximum permeability and selectivity reached up to 910 barrer and 83, thus being superior to most of the state-of-the-art ethylene/ethane separation membranes. Finally, the separation mechanism was revealed, and the regulation of hydrogen-bond and coordinative interactions within DESMs by the rational structural design accounted for excellent performances. This work extends the DES library and will accelerate the prosperity of DESMs for energy-intensive gas separations.

KEYWORDS: deep eutectic solvents, ethylene/ethane, membrane separation, carrier-facilitated transport, structure design, same-anion strategy
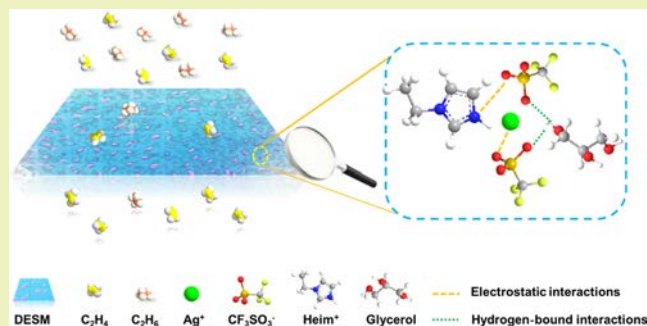
INTRODUCTION

Olefin/paraffin separation is one of the most important separation processes in the chemical industry,[1−5] which can be accomplished by cryogenic distillation, absorptive separation, adsorptive separation, and membrane separation.[6−10] Among all types of separation techniques, membranes with the carrier-facilitated transport mechanism are of great significance and the corresponding membrane performance can be greatly boosted by the elegant design of the membrane matrix and the incorporation of providential carriers, such as silver salts, copper salts, and copper or silver nanoparticles.[11−16] For example, Isabel et al. utilized the polymeric ionic liquid (IL) and IL as the membrane matrix and silver salt as the carrier to carry out ethylene/ethane separation, where the facilitated transport was achieved and the increase of carrier concentration boosted the ethylene solubility, resulting in the high ethylene/ethane selectivity surpassing the upper bound for polymeric membranes.[17] Kang et al. reported of the PEBAX-1657/AgBF$_4$/Al(NO$_3$)$_3$ membrane for olefin/paraffin separation, and the introduction of Al(NO$_3$)$_3$ significantly enhanced the carrier stability.[18] Yang et al. evaluated layered metal−organic framework (MOF) membranes modified with the IL/

AgBF$_4$ composite for ethylene/ethane separation, and the modification converted an inert MOF membrane into an olefin-selective membrane. Despite the great progress made for the development of an advanced membrane matrix based on novel materials as well as the methodologies of manipulation of carrier activity,[19] there is an urgent demand to construct innovative membranes for more effective ethylene/ethane separation.

Recently, deep eutectic solvents (DESs) have emerged as the green and designable solvents and evolved as versatile alternatives for ILs, which are easily prepared by mixing the hydrogen bond acceptor (HBA) and hydrogen bond donor (HBD) at a specific stoichiometric ratio, thus obtaining a much lower eutectic point than the melting temperature of their constituents due to the reconstruction of intermolecular forces
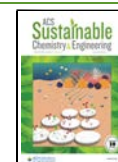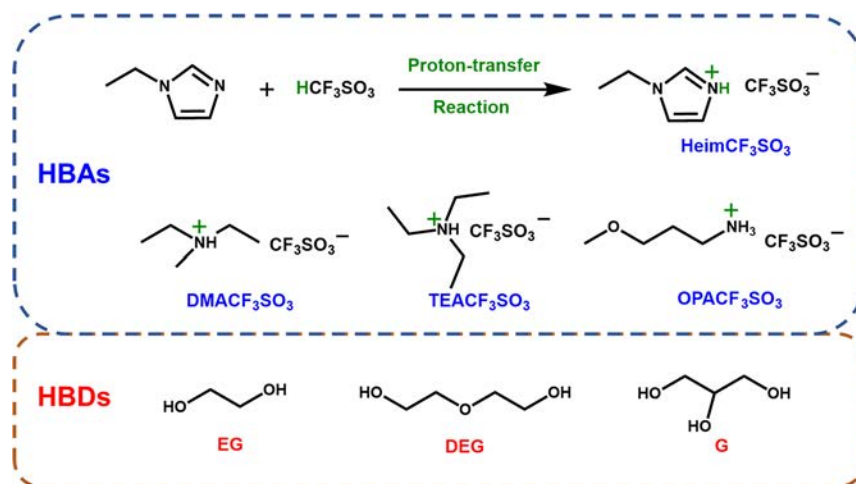
Figure 1. Synthesis of HBAs as well as the chemical structures of HBAs and HBDs for the fabrication of DESs.

during mixing.[20−22] DESs not only inherit the favorable properties of ILs but also foster new features such as low-cost, biodegradability, nontoxicity, and facile fabrication with neither byproduct generation nor need of postpurification,[23] which has been widely applied in energy- and environment-related fields with grand sustainability for gas separation, water filtration, extraction, and batteries.[24−30] However, the application of DESs for the olefin/paraffin membrane separation is still in its infancy. In 2017, for the first time, our group designed CuCl-based DES membranes (DESMs) for ethylene/ethane separation, and the anionic clusters such as $[CuCl_2]^-$ and $[Cu_2Cl_3]^-$ formed between the Cl^- with CuCl acted as the carriers to facilitate ethylene transport, but ethylene permeability and ethylene/ethane selectivity needed to be further enhanced.[31,32] Compared with cuprous salts, silver salts such as $AgCF_3SO_3$ possess more activity to facilitate the transport of ethylene molecules. However, almost all the reported DESs since 2003 contain halide (Cl^- or Br^-) as the anion and easily induce an undesirable precipitation reaction between the silver cation and halide, which creates a great obstacle for the application of DESs as membrane materials to carry out ethylene/ethane separation via a silver carrier-facilitated transport mechanism.[33] In order to overcome this fundamental obstacle, developing novel DESs with an innovative design strategy is highly needed for the simultaneous achievement of high ethylene permeability, ethylene/ethane selectivity, and stability. Moreover, the elucidation of relationship between the structure of DESs and carrier activity is a prerequisite for the forward-looking development of DESMs.

In this study, we proposed the same-anion strategy to prepare novel DESs with the same anion as an ethylene transport carrier ($AgCF_3SO_3$) for the construction of DESMs to carry out ethylene/ethane separation. To the best of our knowledge, the stable DESs with $CF_3SO_3^-$ anions were designed for the first time, and were characterized by ^1H NMR, attenuated total reflection Fourier transform infrared spectroscopy (ATR−FTIR), and differential scanning calorimetry (DSC), revealing the molecular interactions deriving the DES formation. Then, DESMs were fabricated by the impregnation of as-designed DES and $AgCF_3SO_3$ within the porous poly(vinylidene fluoride) (PVDF) membrane by a facile pressure-assisted filtration method, and the membrane morphology was probed by scanning electron microscopy (SEM). The DESMs exhibited high ethylene permeability,

ethylene/ethane selectivity, as well as long-term stability due to the tailorable structure of DES and the proton acidity of as-synthesized HBAs. Moreover, the effects of DES chemical composition and operating conditions on the separation performance were investigated. Finally, separation mechanism was discussed in depth, which turned out that hydrogen-bond interactions as well as the coordination interactions manipulated the gas separation performance and could be tailored by the rational design of the DES structure. The excellent separation performance and good stability made DESMs as a promising alternative to conventional ethylene/ethane separation technologies.

■ EXPERIMENTAL SECTION

Materials. Triethylamine (TEA, >99.5%) and 1-ethylimidazole (Heim, 98%) were sourced by Macklin. N,N-Diethylmethylamine (DMA, >98.0%), 3-methoxypropylamine (OPA, 99%), trifluoromethanesulfonic acid (>99.0%), and silver trifluoromethanesulfonate ($AgCF_3SO_3$, >99.0%) were purchased from Sigma-Aldrich. Methanol (99.5%), ethylene glycol (EG, >99.0%), diethylene glycol (DEG, >99.0%), and glycerol (G, 99.5%) were provided by Heowns. Hydrophilic PVDF support membranes with a pore size of 0.1 μm, porosity of 75%, and average thickness of 100 μm were obtained from Haining Zhongli Filtering Equipment Corporation (China). Nitrogen gas (N_2, 5 N), ethylene (C_2H_4, >99.5%), and ethane (C_2H_6, >99.5%) were supplied by Tianjin Dongxiang Gas Co., LTD (China).

Preparation of DESMs. DESMs were prepared by a pressure-assisted infiltration method.[34] Prior to membrane fabrication, the HBAs and DESs were synthesized (Figure 1, Supporting Information), and $AgCF_3SO_3$−DES mixed solutions with different carrier concentrations were obtained by dissolving the desired amount of $AgCF_3SO_3$ in DES at 60 °C with stirring for 4 h to endure the complete dissolution, followed by cooling to room temperature. Subsequently, the PVDF membrane was kept in a vacuum drying oven at 60 °C for 3 h to remove the trace water from the pores, and $AgCF_3SO_3$−DES mixed solution was uniformly casted on the surface of the PVDF membrane. The solution-casted PVDF membrane was placed in a permeation cell, and the cell was tightened. After that, nitrogen gas was introduced into a permeation cell to improve the cell pressure up to 1 bar, and the mixed solution on the membrane surface was easily pressed into the membrane pores with the assistance of pressure. This procedure was repeated for several times to ensure that the pores were completely occupied by the mixed solution. Finally, DESMs were obtained by removing excess liquid on the membrane surface with nonwoven fabrics and then were used for the gas permeability measurements.
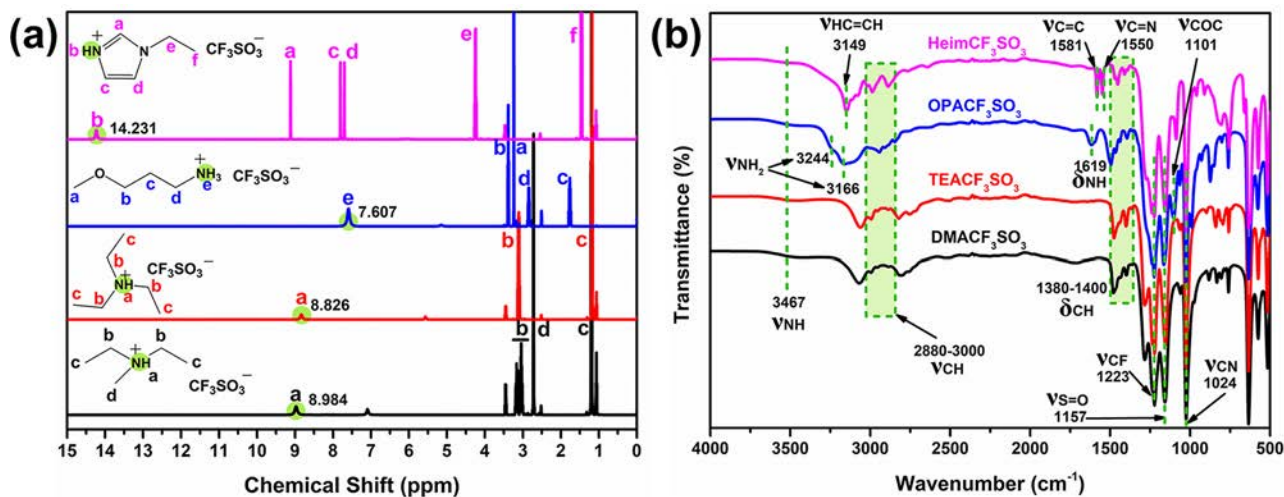
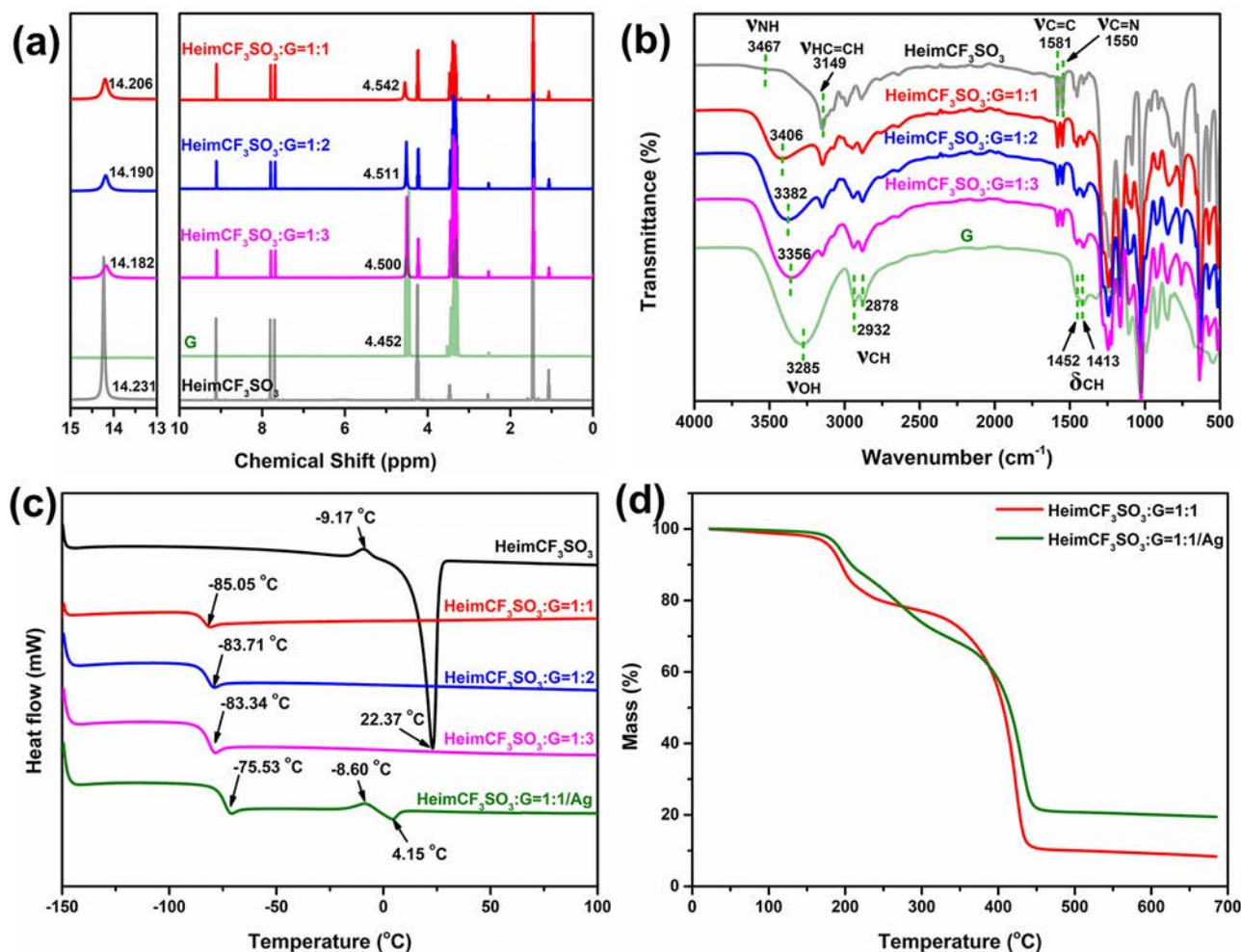**Figure 2.** Successful synthesis of HBAs. (a) ^{1}H NMR. (b) ATR−FTIR spectra.

Figure 3. Investigation of intermolecular interactions driving the DES formation and the thermal properties of DESs. (a) ^{1}H NMR spectra. (b) ATR−FTIR spectra. (c) DSC curves and (d) TG curves of DES and AgCF$_3$SO$_3$−DES mixed solution.

Characterization. ^{1}H nuclear magnetic resonance (^{1}H NMR) spectra were recorded using a VARIA INOVA 500 MHz spectrometer. ATR−FTIR analysis was conducted by a NICOLE-TiS-50 FTIR spectrometer. The DSC experiments were carried out with a TA Instruments Q2000 equipped with cryogenic determination. Thermal decomposition curves were evaluated using a thermal

gravimetric analyzer (NETZSCH TG 209). The surface and cross-section morphologies of the DESMs were observed by field-emission SEM (Hitachi S-4800) and the surface element distribution was recorded by energy-dispersive spectrometry (EDS). The viscosities of the DESs and Ag−DESs at different temperatures were tested by a viscometer (Brookfield LVDV-II + Pro) as the similar procedure in ref

35. The contact angles of the DES and AgCF$_3$SO$_3$−DES mixed solution toward the PVDF support were evaluated by a SL200B/K automatic contact angle meter (America Kino industrial Co., Ltd). More details are included in the Supporting Information.

Gas Permeability Measurements. A homemade apparatus was used for measuring the mixed-gas separation performance (Figure S1), and the procedure is briefly described below and the detail test conditions are seen from the Supporting Information.[36] A freshly prepared DESM was placed in a stainless-steel permeation cell between the feed side and the permeate side with an effective membrane area of 19.625 cm^2. The gas tightness of the apparatus was evaluated by the constant pressure of 2 bar for 1 h. During the gas tightness measurement, no membrane was placed in the permeation cell. After that, the feed gas with an equal molar of C$_2$H$_4$ and C$_2$H$_6$ was introduced to the feed side with the total flow rate 60 mL/min (STP), which was controlled by a mass flow controller with an accuracy of ±0.5%. In the permeate side, nitrogen with a flow rate of 20 mL/min (STP) was used as sweeping gas, and the concentrations of C$_2$H$_4$ and C$_2$H$_6$ in permeation gas were quantified by an online gas chromatography (model GC 2008B, Lunan, equipped with a gas autosampler and a flame ionization detection device) every 10 min. In all experiments, the temperature of the membrane cell was precisely controlled by an air blowing thermostatic oven and the pressure of the feed side was recorded by a pressure transducer. The gas permeability (P_m) through the DESM was calculated according to eq 1

$$P_{m,i} = J_i \times \frac{\delta}{\Delta P_i} \tag{1}$$

where $P_{m,i}$ is the permeability of gas i, barrer {1 barrer = 10^{-10} [cm^3 (STP) cm]/(cm^2 cmHg s)}; J_i is the transmembrane permeation flux, which was calculated as the volume flow of the gas divided by the effective area of the membrane, cm^3/cm^2 s; δ is the membrane thickness (100 μm); and ΔP_i is the partial pressure of the component i between the feed and permeate side, bar. All the experimental data points were the averages of the multiple experimental data, and the standard deviation σ of permeability data was lower than 0.03, concluding that there was a good experimental reliability.

Moreover, the corresponding separation selectivity was calculated according to eq 2

$$\alpha_{i,j} = \frac{P_{m,i}}{P_{m,j}} \tag{2}$$

where i and j are the most and least permeable gases, respectively.

■ RESULTS AND DISCUSSION

Synthesis and Characterization of HBAs. The successful synthesis and chemical structure of HBAs were characterized by ^{1}H NMR and ATR−FTIR spectra. The chemical shifts of active hydrogen of HeimCF$_3$SO$_3$, OPACF$_3$SO$_3$, TEACF$_3$SO$_3$, and DMACF$_3$SO$_3$ appeared at 14.231, 7.607, 8.826, and 8.984 ppm (Figure 2a), respectively, illustrating the occurrence of the proton transfer reaction as well as the successful synthesis of the HBAs. Taking a case of HeimCF$_3$SO$_3$, the presence of chemical shifts at 9.117, 7.806, and 7.702 ppm were attributed to C$_a$−H, C$_c$−H, and C$_d$−H of the imidazole ring, while the chemical shifts at 4.241 and 1.456 ppm were ascribed to C$_e$−H and C$_f$−H in the alkyl side chain. The chemical structures of the HBAs were further explored by ATR−FTIR (Figure 2b). In the spectrum of HeimCF$_3$SO$_3$, the characteristic peak at 3467 cm^{-1} corresponded to the symmetrical stretching vibration of N−H and the characteristic peak at 3149 cm^{-1} was assigned to the =CH stretching vibration. The peaks in the range of 2880−3000 and 1380−1400 cm^{-1} were contributed to the stretching vibrations and bending vibrations of C−H. Three characteristic peaks located at 1581, 1550, and 1024 cm^{-1} deriving from stretching

vibration of C=C, C=N, and C−N stretching vibrations, respectively, which confirmed the chemical structure of the cation in HeimCF$_3$SO$_3$. Meanwhile, the CF$_3$SO$_3$$^-$ anion was marked as peaks at around 1223 and 1157 cm^{-1} due to C−F and S=O stretching vibrations.

Design and Characterization of the DESs. The intermolecular interactions driving the DES formation were investigated by ^{1}H NMR and ATR−FTIR spectra. As shown in Figure 3a, the chemical shift at 14.23 ppm in the ^{1}H NMR spectrum of HeimCF$_3$SO$_3$ was attributed to N−H of the imidazolium cation, and it gradually shifted to upfield with the decrease of the HeimCF$_3$SO$_3$/G molar ratio, which were 14.206 to 14.182 ppm for molar ratios of 1:1 and 1:3, indicating the destruction of ionic hydrogen-bond interactions and electrostatic interactions between the cation and anion of HeimCF$_3$SO$_3$ by the insertion of G. Additionally, the improved peak width of N−H suggested the newly formed hydrogen-bond interactions between HeimCF$_3$SO$_3$ and G. The OH chemical shift of G at 4.452 ppm shifted to down-field after mixing with HeimCF$_3$SO$_3$ and gradually shifted to upfield from 4.542 to 4.500 ppm with the decrease of the HeimCF$_3$SO$_3$/G molar ratio from 1:1 to 1:3, which was attributed to the stronger newly formed hydrogen-bond interactions between HeimCF$_3$SO$_3$ and G in relative to that between G and G. The intermolecular interactions between HBA and HBD were also confirmed by the ATR−FTIR spectra (Figure 3b). The ATR−FTIR spectra of DESs exhibited the characteristic peaks of both HeimCF$_3$SO$_3$ and G, and the DESs with different molar ratios exhibited similar spectra due to the close resemblance of their chemical structures. Methyl groups were marked at around 2932, 2878, 1452, and 1413 cm^{-1} due to the C−H stretching vibration and C−H bending. The broad peak between 3350 and 3610 cm^{-1} was the overlapping between the O−H stretching vibration band of G and the N−H stretching vibration band of HeimCF$_3$SO$_3$, which suffered from red shifts from 3406 to 3356 cm^{-1} with the HeimCF$_3$SO$_3$/G molar ratio changing from 1:1 to 1:3, indicating the tunable hydrogen-bond interactions with different molar ratios. The strong hydrogen-bond interactions between HeimCF$_3$SO$_3$ and G induced the charge-delocalization of the cation and anion, which significantly weakened the electrostatic interactions, thus forming stable and homogeneous DESs.

The thermal properties of DESs were analyzed by DSC and TG curves. As seen from Figure 3c, a cold recrystallization peak at −9.17 °C and a melting peak at 22.37 °C were observed for HeimCF$_3$SO$_3$. As for DESs, only a glass transition temperature (T_g) at a very low temperature was identified without any cold recrystallization and melting peak, which was a characteristic trait of DESs. The insertion of G into HeimCF$_3$SO$_3$ destroyed the long-range ordered structure between the anion and cation in HeimCF$_3$SO$_3$, thus hindering the crystallization of HeimCF$_3$SO$_3$ and causing the disappearance of the melting point. The T_g raised from −85.05 to −83.34 °C with the decrease of HeimCF$_3$SO$_3$/G. After the dissolution of AgCF$_3$SO$_3$, T_g obviously increased up to −75.53 °C due to the introduction of strong cation−anion electrostatic interactions.[37] Moreover, a cold recrystallization peak at −8.60 °C and a melting peak at 4.15 °C appeared, which suggested the liberation of few HeimCF$_3$SO$_3$ from hydrogen-bond networks between HeimCF$_3$SO$_3$ and G due to the competitive interactions between AgCF$_3$SO$_3$ and G.[38,39] However, these two peaks were extremely weak, and the melting point of AgCF$_3$SO$_3$−DES was significantly lower than that of
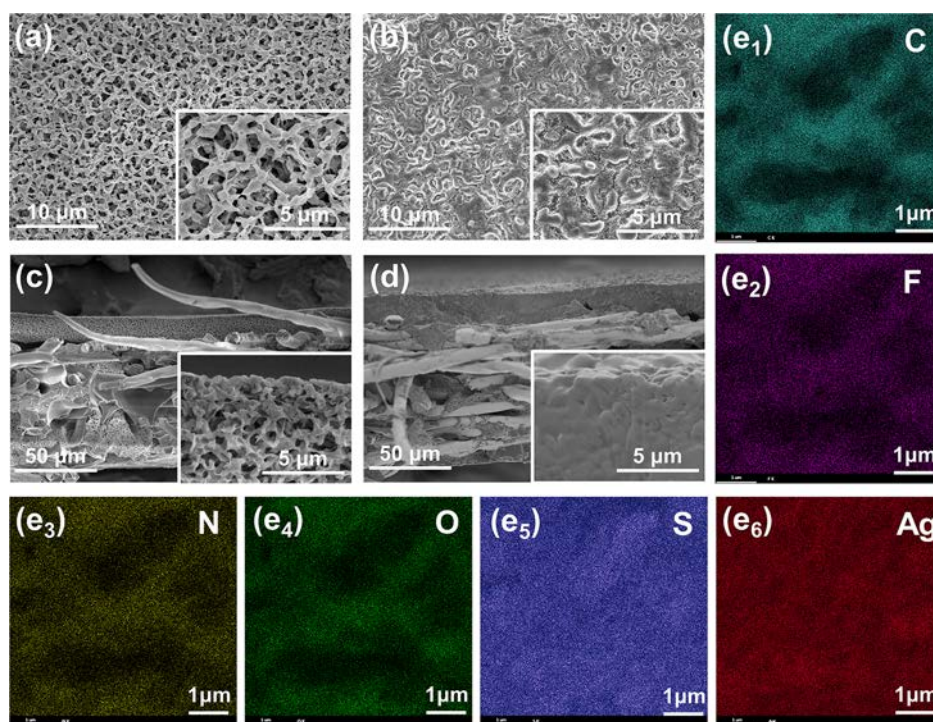
Figure 4. Surface and cross-sectional SEM images of the (a,c) PVDF support and (b,d) [HeimCF$_3$SO$_3$][G]-based DESM. (e) EDS mapping of [HeimCF$_3$SO$_3$][G]-based DESM.
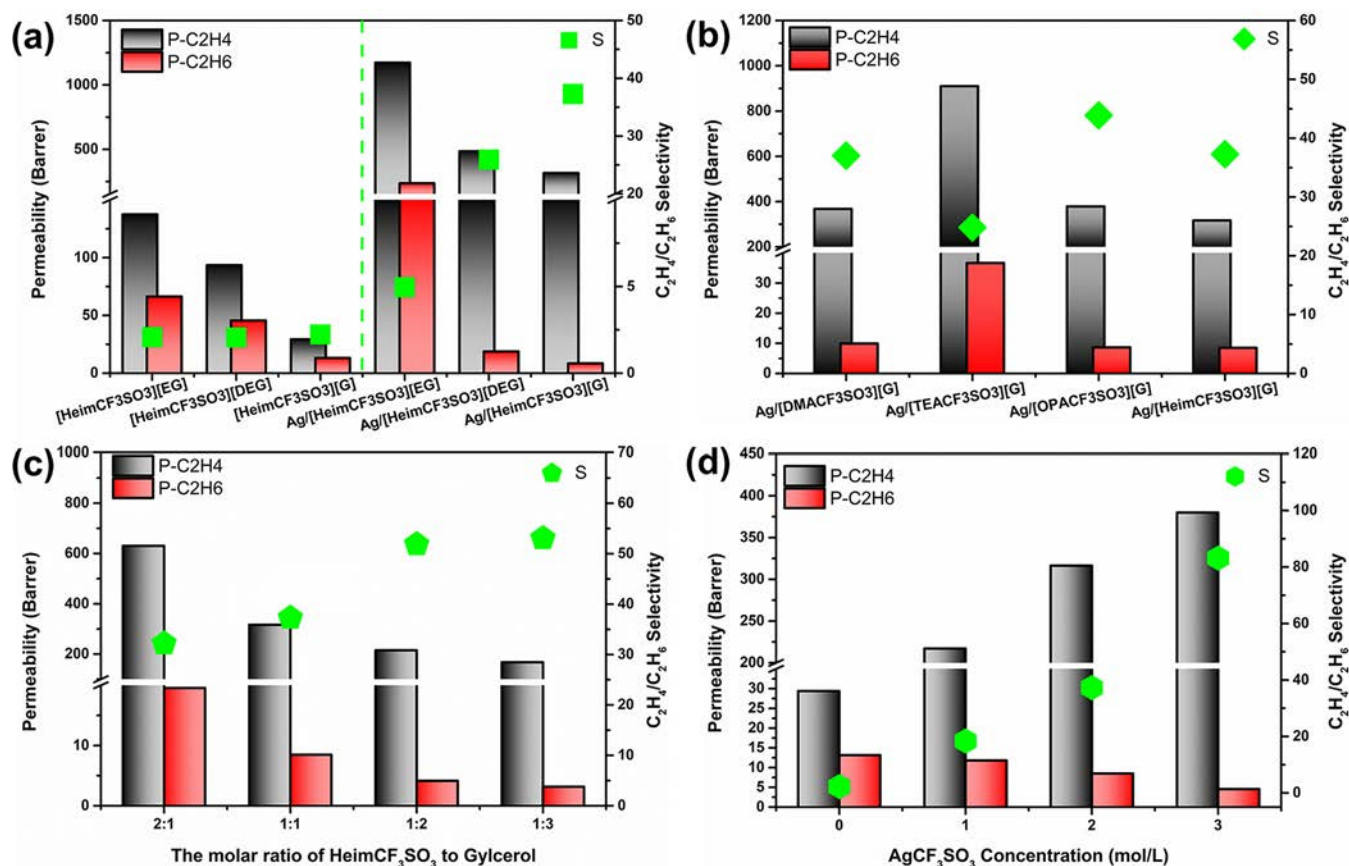
Figure 5. Separation performance of DESMs. (a) The effect of HBDs, (b) the effect of HBAs, (c) the effect of molar ratio of HeinCF$_3$SO$_3$ to G, and (d) the effect of AgCF$_3$SO$_3$ concentration. The test conditions: AgCF$_3$SO$_3$ concentration of 2 mol/L, the molar ratio of HBA to HBD of 1:1, the pressure of 0.1 bar, the temperature of 25 °C, and the gas flow rate of 60 mL/min (STP) with equal molar of C$_2$H$_4$ and C$_2$H$_6$.

HeimCF$_3$SO$_3$, which indicated that the nature of DES was not broken. Finally, the TG analysis of DES displayed a two-stage decomposition and showed thermal stability up to 180 °C, while the three-stage decomposition was presented and the rate of thermal decomposition slowed down for AgCF$_3$SO$_3$–DES, indicating the generation of new interactions and the enhancement of thermal stability upon the addition of AgCF$_3$SO$_3$ (Figure 3d). The TG curves confirmed the satisfactory thermal stability, which indicated the good thermal stability of the resultant DESMs.

Morphological Study of DESMs. The microstructure of DESMs was examined by SEM. As seen from Figure 4a, the PVDF support showed the randomly distributed macroporous on the surface, and the pore sizes were estimated to be 200 nm to 1 μm. The cross-sectional images revealed the typical three-layered structure of the PVDF support: the top and bottom surface layers owned interconnected hierarchical porous with the thickness of about 20 μm, which ensured the continuous distribution of the solution; and the interlayer consisting of penetrated fibers was designed to provide sufficient mechanical support (Figure 4c). After impregnation of AgCF$_3$SO$_3$–DES mixed solution into the PVDF support under positive capillary force, the macroporous were homogeneously filled and no obvious cracks or defects can be found (Figure 4b). The cross-sectional images in Figure 4d also revealed that the interconnected hierarchical porous were completely occupied by the AgCF$_3$SO$_3$–DES mixed solution, indicating the good compatibility between the mixed solution and PVDF support. The contact angle of AgCF$_3$SO$_3$–DES mixed solution on the hydrophilic PVDF membrane was 58.9°, which further suggested good compatibility and wettability of DESs toward the support, thus creating a favorable prerequisite for the fabrication of stable DESMs (Figure S2). Moreover, the element distribution of DESM was further explored by EDS mapping images (Figure 4e), and the elements of C, F, N, O, S, and Ag were detected and uniformly distributed on the surface of the membrane, further confirming the successful preparation of the DESMs.

Separation Performance of DESMs. *Effect of HBDs.* The performances of DESMs with or without the AgCF$_3$SO$_3$ carrier for C$_2$H$_4$/C$_2$H$_6$ separation were evaluated (Figure 5). The DESMs without the carrier exhibited a C$_2$H$_4$ permeability lower than 200 barrer and the extremely low C$_2$H$_4$/C$_2$H$_6$ selectivity of 2, which could barely achieve the selective separation (Figure 5a). Without carriers, gas permeation through the DESMs heavily relied on the solution-diffusion mechanism, and the similarity of C$_2$H$_4$ and C$_2$H$_6$ physical properties resulted in a small difference of both solubility and diffusivity. Regarding to the DESMs with a carrier, both C$_2$H$_4$ permeability and C$_2$H$_4$/C$_2$H$_6$ selectivity increased dramatically, which was attributed to the attendance of the carrier-facilitated transport mechanism. The disassociated silver ion coordinated with ethylene to form the complex [Ag(C$_2$H$_4$)$_x$]$^+$, which significantly accelerated the transmembrane transport of ethylene molecules. As a result, the C$_2$H$_4$ permeability of [HeimCF$_3$SO$_3$][G]-based DESM increased from 29 to 316 barrer, corresponding to a maximum enhancement of 1090%. Meanwhile, the C$_2$H$_4$/C$_2$H$_6$ selectivity significantly increased up to 37. As also revealed by Figure 5a, the effect of HBD on C$_2$H$_4$ permeability followed the order: EG > DEG > G, while C$_2$H$_4$/C$_2$H$_6$ selectivity witnessed an inverse trend. The DESM with G or DEG as HBD obtained low C$_2$H$_6$ permeability, which was much lower compared with DESM without carrier,

resulting in high C$_2$H$_4$/C$_2$H$_6$ selectivity. In contrast, the DESMs with EG as HBD obtained low C$_2$H$_4$/C$_2$H$_6$ selectivity due to the high C$_2$H$_6$ permeability, which significantly increased from 66 to 236 barrer with the addition of AgCF$_3$SO$_3$. The high C$_2$H$_6$ permeability of EG-based DESMs was probably attributed to the loose structure of DESs induced by the incorporation of AgCF$_3$SO$_3$. The EG-based DESMs have a weak hydrogen-bond network and the incorporation of AgCF$_3$SO$_3$ further damaged the hydrogen-bond network, which resulted in a loose structure with high chain flexibility, thus contributing to high C$_2$H$_6$ permeability.[19,31] Finally, considering the good comprehensive performance in terms of both C$_2$H$_4$ permeability and C$_2$H$_4$/C$_2$H$_6$ selectivity, as well as the biodegradable, low toxicity, cheap, and nonflammable characteristics of G,[40−42] the [HeimCF$_3$SO$_3$][G]-based DESM was used as a prototype for further investigation.

Effect of HBAs. DESMs fabricated with four different HBAs were obtained to investigate the effect of HBAs on the separation performance, which confirmed that the gas separation performances could be tailored by the chemical structure of HBAs such as molecular size and functional group (Figure 5b). The [TEACF$_3$SO$_3$][G]-based DESM obtained an extremely high C$_2$H$_4$ permeability of 910 barrer and a moderate C$_2$H$_4$/C$_2$H$_6$ selectivity of 25, while [DMACF$_3$SO$_3$]-[G]-based DESM exhibited a C$_2$H$_4$ permeability of 390 barrer and a high C$_2$H$_4$/C$_2$H$_6$ selectivity of 36, which suggested that the larger cation size of HBA resulted in higher C$_2$H$_4$ permeability but lower C$_2$H$_4$/C$_2$H$_6$ selectivity. The smaller size cation generated the stronger electrostatic interactions, which resulted in a more compact structure with the solid arrangement of anions and cations in the DES, thus impeding gas permeation.[43] [HeimCF$_3$SO$_3$][G]-based DESM exhibited a slight lower permeability of 316 barrer and a similar selectivity of 37 in relative to [DMACF$_3$SO$_3$][G]-based DESM, which further highlighted the important effect of HBAs on the performances. [OPACF$_3$SO$_3$][G]-based DESM obtained the maximum C$_2$H$_4$/C$_2$H$_6$ selectivity of 44 and high C$_2$H$_4$ permeability of 395 barrer, which was much better than that of [TEACF$_3$SO$_3$][G]-based DESM, suggesting the facile enhancement of separation performance by the introduction of a functional group. The ether group in the cation of OPACF$_3$SO$_3$ probably afforded the coordinative interactions between Ag$^+$ and C−O−C, which availably promoted the disassociation and activation of silver salt, thus enhancing the transport of C$_2$H$_4$.[44]

Effect of Molar Ratio of HBA and HBD. The separation performances of DESMs with a varied molar ratio of HeimCF$_3$SO$_3$ and G were also evaluated to investigate the impact of the molar ratio of HBA and HBD. As reported in Figure 5c, both C$_2$H$_4$ permeability and C$_2$H$_6$ permeability diminished remarkably as the molar ratio of HeimCF$_3$SO$_3$ and G dropping from 2:1 to 1:3 with the C$_2$H$_4$ permeability from 630 to 168 barrer and C$_2$H$_6$ permeability from 20 to 3 barrer, respectively. However, the C$_2$H$_4$/C$_2$H$_6$ selectivity remained steady enhancement from 32 to 53 with the decrease of molar ratio. Therefore, the different combinations of C$_2$H$_4$ permeability and C$_2$H$_4$/C$_2$H$_6$ selectivity could be obtained by tailoring the molar ratio of HBA to HBD.

Effect of AgCF$_3$SO$_3$ Concentration. The effect of the AgCF$_3$SO$_3$ concentration on the separation performances of DESMs is reported in Figure 5d, raising the AgCF$_3$SO$_3$ concentration in the DESMs led to a conspicuous improve-
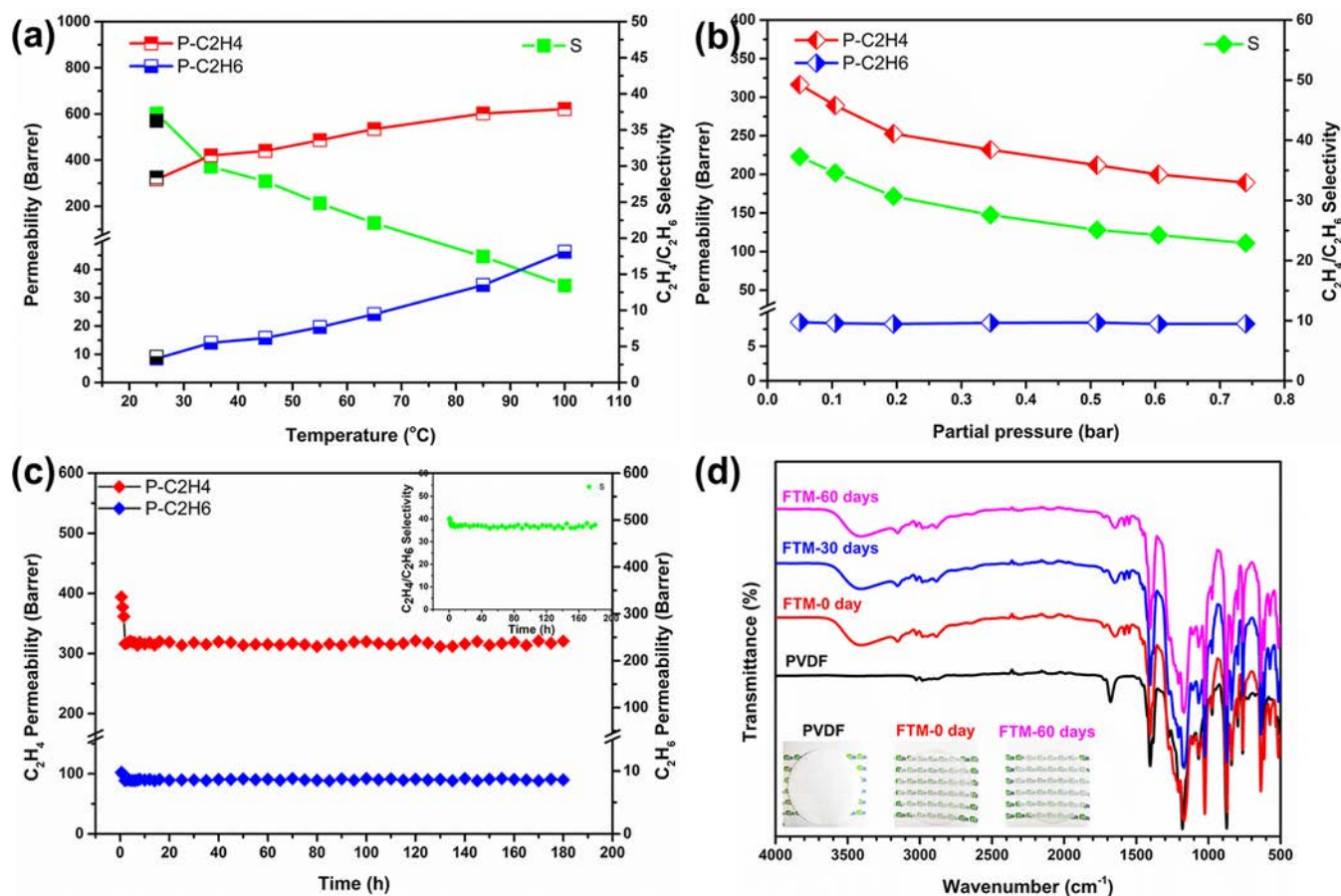
Figure 6. Effects of (a) temperature and (b) pressure on the separation performance of $[HeimCF_3SO_3][G]$-based DESM. (c) The operational stability and (d) chemical stability of $[HeimCF_3SO_3][G]$-based DESM. Note: the black dots in Figure 6a presented the results with the turned down of the temperature to 25 °C after the heating process. The $AgCF_3SO_3$ concentration was kept at 2 mol/L and the molar ratio of HBD and HBA was 1:1. Test conditions: the pressure of 0.1 bar, the temperature of 25 °C, and the gas flow rate of 60 mL/min (STP) with an equal molar of C_2H_4 and C_2H_6 unless otherwise stated. The temperature ranged from 25 to 100 °C during the investigation of the effect of temperature, and the pressure ranged from 0.1 to 1.5 bar during the investigation of the effect of pressure.

ment of the C_2H_4/C_2H_6 selectivity, which increased from 2 to 83 with the increase of $AgCF_3SO_3$ concentration from 0 to 3 mol/L. Meanwhile, the C_2H_4 permeability witnessed a nearly linear increase with the increase of silver salt concentration and reached up to 380 barrer at 3 mol/L. In contrast, C_2H_6 permeability decreased prominently, and the different trends of C_2H_4 and C_2H_6 permeability were mainly attributed to the different transport mechanisms. As for C_2H_4 permeability based on the carrier-facilitated transport mechanism, the increase of $AgCF_3SO_3$ concentration conferred the DESMs with more effective carriers to selectively transport C_2H_4 molecules. However, the C_2H_6 permeability solely depended on the solution-diffusion mechanism, and the addition of more silver salt did not enhance the diffusion of C_2H_6 molecules and decreased C_2H_6 solubility due to the ubiquitous salting-out effect, thus resulting in the gradual decrease of C_2H_6 permeability.

Effect of Operation Conditions. The operation conditions such as operating temperature and pressure also played an important role on the separation performance of DESMs (Figure 6). It was found that the temperature triggered simultaneous improvements on C_2H_4 permeability and C_2H_6 permeability, while the selectivity of C_2H_4/C_2H_6 exhibited a distinct decline from 37 to 13 (Figure 6a). For example, the C_2H_4 permeability increased by nearly 2 times (from 316 to

622 barrer), and the C_2H_6 permeability increased by above five times (from 8 to 46 barrer), which was explained by the improvement of gas diffusion induced by the increase of the temperature. The viscosities of Ag−DESs decreased with the increase of the temperature, which contributed to fast gas diffusion (Table S1). However, the increase of temperature weakened the complexation between Ag^+ and C_2H_4, which diminished the carrier-facilitated transport of C_2H_4 molecules, resulting in a slower increase of C_2H_4 permeability in relative to C_2H_6 permeability. The separation performance of the $[HeimCF_3SO_3][G]$-based DESM almost remained unchanged after turning the temperature back to 25 °C, indicating the excellent thermal stability of the DESMs. As shown in Figure 6b, the C_2H_6 permeability indicated no dependency on pressure and remained almost unchanged.[45] Meanwhile, the C_2H_4 permeability experienced a moderate decrease from 316 to 189 barrer as the pressure increased from 0.1 to 0.74 bar, which was a feature of the carrier-facilitated transport mechanism due to the carrier saturation even at low pressure.[43,44] As a result, the C_2H_4/C_2H_6 selectivity decreased from 37 to 23.

Stability of DESM. The $[HeimCF_3SO_3][G]$-based DESM was continuously operated for 1 week to demonstrate the stability of DESMs (Figure 6c). The gas permeability and C_2H_4/C_2H_6 selectivity experienced a sharp decrease during the

first 2 h, which was probably caused by the increased viscosity of the $AgCF_3SO_3$−DES mixed solution due to the evaporation of water.[46−48] After that, both C_2H_4 permeability and C_2H_4/ C_2H_6 selectivity fluctuated slightly in a narrow range, confirming a stable performance in the long-term test. In addition, the membrane was removed from the permeation cell and kept under ambient condition for 2 months without any protection, and ATR−FTIR spectra were recorded once a month to study the chemical stability of DESMs. The ATR− FTIR spectra of DESM remained almost unchanged with time and the membrane was still transparent and colorless (Figure 6d), which indicated no appearance of black reduced silver particles, further confirming the stability of DESMs. The good stability could be traced back to the protonic acidic property of HBA, which effectively stabilized the Ag^+ carrier.

Comparison with Other Studies. The C_2H_4/C_2H_6 separation performances of as-developed DESMs in this work were compared with previously reported C_2H_4/C_2H_6 separation membranes, including conventional polymeric membranes, carbon molecular sieve (CMS) membranes, mixed matrix membranes (MMMs), MOF membranes, polymeric carrier-facilitated transport membranes (FTMs), IL membranes, and DESMs (Figure 7). The values of gas
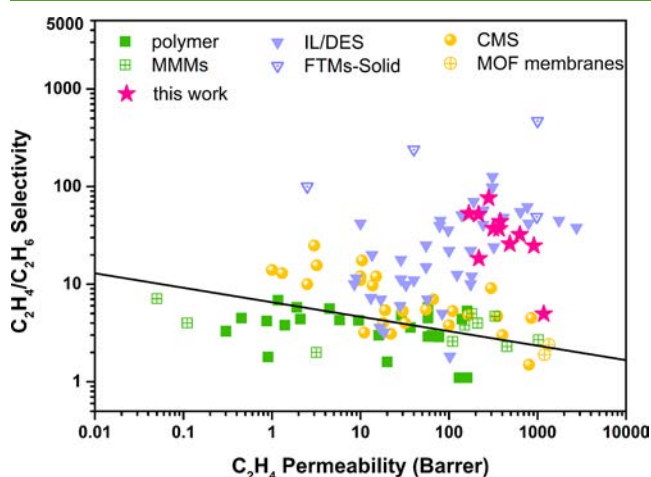

Figure 7. Performance comparison of the DESMs in this work with other membranes reported in literatures for C_2H_4/C_2H_6 separation.

permeability and selectivity, and the corresponding membrane materials, membrane thickness, test method, and test conditions have also been collected in Table S2 in the Supporting Information. Obviously, the DESMs exhibited the excellent comprehensive separation performance with respect to both C_2H_4 permeability and C_2H_4/C_2H_6 selectivity, which surpassed the 2013 upper bound for polymer membranes. The separation performances of DESMs outperformed MMMs based on the solution-diffusion mechanism and were also much better than CMS membranes and MOF membranes based on the molecular sieving mechanism.[49] DESMs were better than or comparable with most of advanced IL and DES based membranes based on carrier-facilitated transport mechanism. Compared with solid FTMs operated under wetted feed condition, the DESMs were easily operated with no need humidification of feed gas. Considering the facile membrane fabrication and charming features of DESs, the DESMs are promising for C_2H_4/C_2H_6 separation. However, for the real industrial application of DESMs, more efforts are

needed. First, the preparation of defect-free ultrathin DESMs is the first step, and hollow fiber membrane contactors or the bulk flowing hollow fiber membrane contactors are preferential.[50] Second, the DESMs cannot tolerate high pressure and process optimization is needed for their industrialization; finally, although DESMs exhibit good stability under the ambient condition without any protection, their long-term membrane performances under real feeds of ethylene, ethane, H_2, C_2H_2, and H_2S are still needed.[9,18,51] Moreover, the pretreatment of mixed gas to eliminate C_2H_2 and H_2S contaminants before membrane separation is also a reliable choice for the sake of long-term membrane stability.

Separation Mechanisms. Regrading the separation mechanism of DESMs, it is widely accepted that the C_2H_6 permeability only relies upon Fick diffusion, while C_2H_4 permeability mainly depends on the carrier-facilitated transport mechanism, which is closely associated with carrier activity. The carrier activity was mainly determined by the molecular interactions between the silver salt carrier and DESs, which was investigated by ^1H NMR and ATR−FTIR spectra. As shown in Figure 8a, with the introduction of $AgCF_3SO_3$ into the DESs, the OH chemical shift of G increased from 4.542 to 4.546 ppm, from 4.511 to 4.513 ppm, and from 4.500 to 4.526 ppm with the molar ratios of $HeimCF_3SO_3$ and G at 1:1, 1:2, and 1:3, respectively, which indicated the hydrogen-bond interactions between $CF_3SO_3^-$ of silver salt and HBDs. In the ATR−FTIR spectra (Figure 8b), the peaks at 1223 and 1157 cm^{-1} representing the C−F stretching and S=O stretching in the $CF_3SO_3^-$ anion showed red shifts after the addition of $AgCF_3SO_3$ into DESs with different molar ratios of $HeimCF_3SO_3$ and G, further confirming the enhancement of the hydrogen-bond interactions between the $CF_3SO_3^-$ anion and G. In contract, the OH stretching vibrations of G exhibited blue shifts, moving from 3406 to 3417 cm^{-1}, from 3382 to 3386 cm^{-1}, and from 3356 to 3383 cm^{-1} as the molar ratio changed from 1:1 to 1:3, indicating the coordination interactions between G and Ag^+. The lone pair electrons of the oxygen on the hydroxyl group paired with the empty outer orbital of the silver ion, which resulted in a reduction of the proportion of G involved in hydrogen-bond interactions. In a word, the hydrogen-bond interactions between $CF_3SO_3^-$ of silver salt and HBDs and the coordination interactions between Ag^+ and HBDs impaired the interactions between Ag^+ and $CF_3SO_3^-$ and effectively promoted the dissociation of $AgCF_3SO_3$, which increased the number of effective carriers and significantly improved the activity of carriers. Similar results have been reported for polymeric electrolyte membranes, where carrier activity can be enhanced by the functional groups of polymers because of coordination interactions, such as ester, ketone, amide, hydroxyl, and ether.[52−55] Therefore, with the increase of the G content, the activity of the carrier was enhanced, which contributed to the increase of C_2H_4/C_2H_6 selectivity. However, when coordination interactions between Ag^+ and OH were too strong, the positive charge density of silver ions would be reduced, which weakened the coordination ability between silver ions and C_2H_4, thus decreasing the facilitated transport of C_2H_4.[56] The ^1H NMR spectra further confirmed hydrogen-bond interactions (Figure 8c). Moreover, in the ATR−FTIR spectra (Figure 8d), the [HeimCF$_3$SO$_3$][DEG]-based DES exhibited a bigger shift than [HeimCF$_3$SO$_3$][G]-based DES, which implied the stronger coordination interactions. Therefore, the

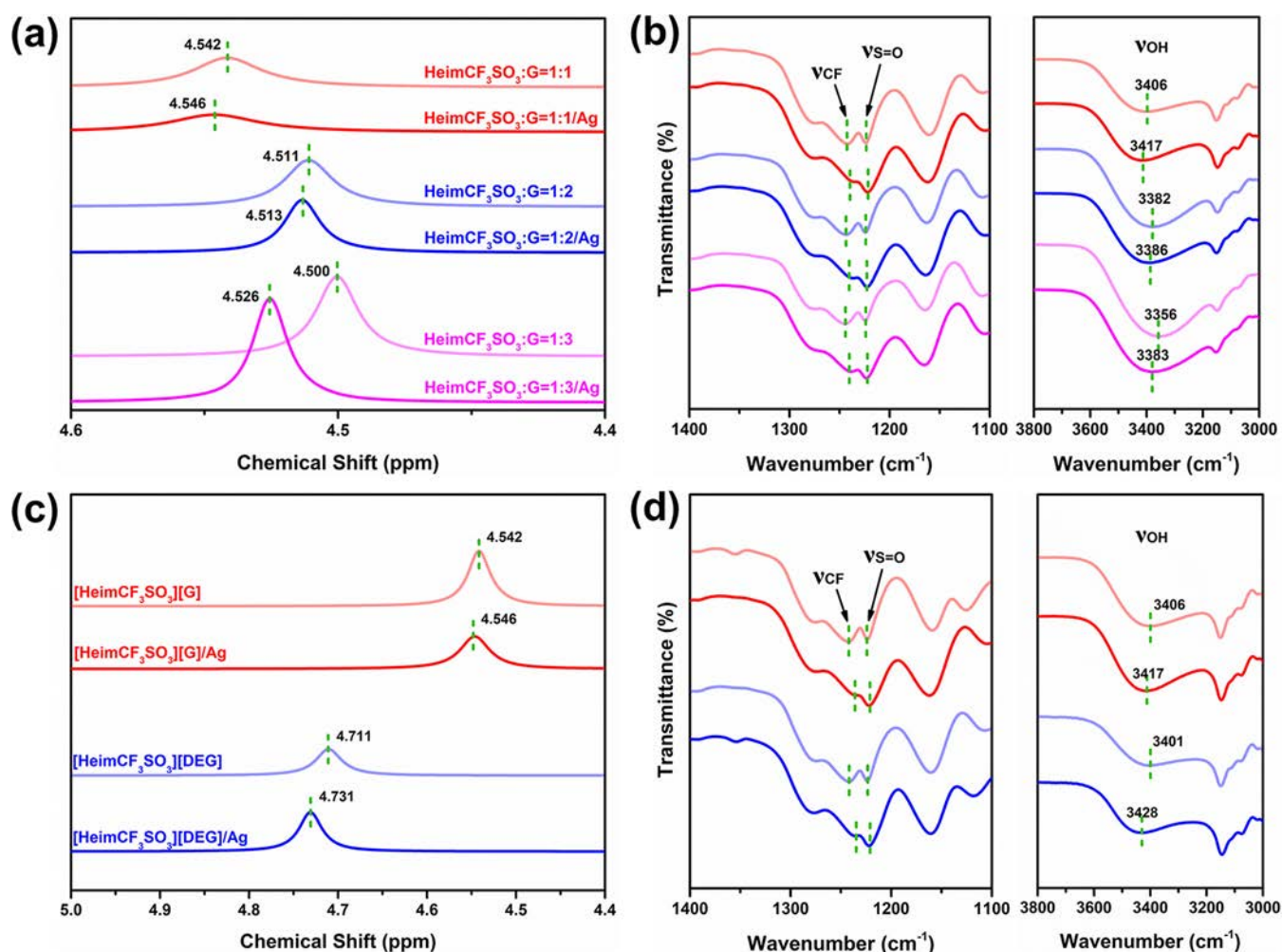**Figure 8.** ^{1}H NMR and ATR–FTIR spectra of DES and DESMs. (a,b) $[HeimCF_3SO_3][G]$ based DES with different molar ratios of HBA and HBD. (c,d) DES with different HBDs (the molar ratio of HBA and HBD was set at 1:1).

$[HeimCF_3SO_3][G]$-based DESM exhibited better separation performance than $[HeimCF_3SO_3][DEG]$-based DESM.

CONCLUSIONS

In summary, novel DESs with $CF_3SO_3^-$ were synthesized for the first time by the same-anion strategy, and a series of DESMs were fabricated to carry out the C_2H_4/C_2H_6 separation, where both C_2H_4 permeability and C_2H_4/C_2H_6 selectivity could be easily tailored by skillful selection of the HBDs, HBAs, and the molar ratios of HBA and HBD. The C_2H_4/C_2H_6 selectivity of DESMs could be significantly improved by adopting smaller-sized HBA or HBA with functional groups, utilizing HBD of G, reducing the molar ratio of HBA and HBD. For example, $[OPACF_3SO_3][G]$-based DESM with the ether bond obtained the maximum C_2H_4/C_2H_6 selectivity of 44 and high C_2H_4 permeability of 395 barrer. Compared with other HBDs, G-based DESMs were more competitive due to the biodegradable, low toxicity, cheap, and nonflammable characteristics of G. In addition, the increase of silver salt concentration also enhanced the separation performances, and a high selectivity of 83 was obtained. The optimization of operation conditions suggested that the decrease of the operating temperature afforded high selectivity but low C_2H_4 permeability, while the decrease of pressure contributed to high selectivity and permeability

simultaneously. The DESM exhibited an excellent operational stability during the change of operating temperature and long-term tests as well as good chemical stability. Finally, the separation mechanism was revealed that the hydrogen-bond interactions between the anion of silver salt and HBD and the coordination interactions between Ag^+ and HBD can effectively improve the activity of the carriers, thus effectively facilitating the transport of C_2H_4. The newly developed DESs with the $CF_3SO_3^-$ anion broadened the range of DESs, and the proposed same-anion strategy opens a new avenue to construct highly efficient and stable DESMs with a silver salt carrier.

ASSOCIATED CONTENT

ⓈI Supporting Information

The Supporting Information is available free of charge at

https://pubs.acs.org/doi/10.1021/acssuschemeng.2c00253.

> Synthesis; characterization; gas permeability measurement; contact angles and viscosities of DESs and Ag–DESs; and details on the comparison of separation performances (PDF)

■ AUTHOR INFORMATION

Corresponding Authors

Na Yang − *School of Chemical Engineering and Technology, Tianjin University, Tianjin 300072, China;* ⊙ orcid.org/0000-0003-4888-5971; Email: yangnayna@tju.edu.cn

Luhong Zhang − *School of Chemical Engineering and Technology, Tianjin University, Tianjin 300072, China;* ⊙ orcid.org/0000-0002-7073-4793; Email: zhanglvh@tju.edu.cn

Authors

Mi Xu − *School of Chemical Engineering and Technology, Tianjin University, Tianjin 300072, China*

Haozhen Dou − *School of Chemical Engineering and Technology, Tianjin University, Tianjin 300072, China;* ⊙ orcid.org/0000-0002-1461-4578

Yanxiong Ren − *School of Chemical Engineering and Technology, Tianjin University, Tianjin 300072, China*

Feifei Peng − *School of Chemical Engineering and Technology, Tianjin University, Tianjin 300072, China*

Xiaoming Xiao − *School of Chemical Engineering and Technology, Tianjin University, Tianjin 300072, China*

Xiaowei Tantai − *School of Chemical Engineering and Technology, Tianjin University, Tianjin 300072, China*

Yongli Sun − *School of Chemical Engineering and Technology, Tianjin University, Tianjin 300072, China*

Bin Jiang − *School of Chemical Engineering and Technology, Tianjin University, Tianjin 300072, China*

Complete contact information is available at:
https://pubs.acs.org/10.1021/acssuschemeng.2c00253

Author Contributions

M.X. synthesized the DESs and performed gas separation measurements. H.D. performed the analysis of ^{1}H NMR and ATR−FTIR spectroscopy. Y.R. measured DSC and TG. F.P. performed SEM analysis. X.X. measured viscosities. X.T. measured contact angles. Y.S., B.J., N.Y., and L.Z. provided fund support and oversaw the experiments and analysis. All authors contributed to the writing and revise of the manuscript.

Notes

The authors declare no competing financial interest.

■ REFERENCES

(1) Su, Y.; Cong, S.; Shan, M.; Zhang, Y. Enhanced propylene/propane separation in facilitated transport membranes containing multisilver complex. *AIChE J.* **2022**, *68*, No. e17410.

(2) James, J. B.; Wang, J.; Meng, L.; Lin, Y. S. ZIF-8 Membrane Ethylene/Ethane Transport Characteristics in Single and Binary Gas Mixtures. *Ind. Eng. Chem. Res.* **2017**, *56*, 7567−7575.

(3) Chen, G.; Chen, X.; Pan, Y.; Ji, Y.; Liu, G.; Jin, W. M-gallate MOF/6FDA-polyimide mixed-matrix membranes for C_2H_4/C_2H_6 separation. *J. Membr. Sci.* **2021**, *620*, 118852.

(4) Qiu, W.; Xu, L.; Liu, Z.; Liu, Y.; Arab, P.; Brayden, M.; Martinez, M.; Liu, J.; Roy, A.; Koros, W. J. Surprising olefin/paraffin separation performance recovery of highly aged carbon molecular sieve hollow fiber membranes by a super-hyperaging treatment. *J. Membr. Sci.* **2021**, *620*, 118701.

(5) Wang, S.; Yang, L.; He, G.; Shi, B.; Li, Y.; Wu, H.; Zhang, R.; Nunes, S.; Jiang, Z. Two-dimensional nanochannel membranes for molecular and ionic separations. *Chem. Soc. Rev.* **2020**, *49*, 1071−1089.

(6) Dou, H.; Xu, M.; Wang, B.; Zhang, Z.; Wen, G.; Zheng, Y.; Luo, D.; Zhao, L.; Yu, A.; Zhang, L.; Jiang, Z.; Chen, Z. Microporous framework membranes for precise molecule/ion separations. *Chem. Soc. Rev.* **2021**, *50*, 986−1029.

(7) Hou, J.; Liu, P.; Jiang, M.; Yu, L.; Li, L.; Tang, Z. Olefin/paraffin separation through membranes: from mechanisms to critical materials. *J. Mater. Chem. A.* **2019**, *7*, 23489−23511.

(8) Ren, Y.; Liang, X.; Dou, H.; Ye, C.; Guo, Z.; Wang, J.; Pan, Y.; Wu, H.; Guiver, M. D.; Jiang, Z. Membrane-Based Olefin/Paraffin Separations. *Adv. Sci.* **2020**, *7*, 2001398.

(9) Campos, A. C. C.; dos Reis, R. A.; Ortiz, A.; Gorri, D.; Ortiz, I. A Perspective of Solutions for Membrane Instabilities in Olefin/Paraffin Separations: A Review. *Ind. Eng. Chem. Res.* **2018**, *57*, 10071−10085.

(10) Park, S.; Jeong, H.-K. Transforming polymer hollow fiber membrane modules to mixed-matrix hollow fiber membrane modules for propylene/propane separation. *J. Membr. Sci.* **2020**, *612*, 118429.

(11) Yang, K.; Ban, Y.; Yang, W. Layered MOF membranes modified with ionic liquid/AgBF$_4$ composite for olefin/paraffin separation. *J. Membr. Sci.* **2021**, *639*, 119771.

(12) Dou, H.; Jiang, B.; Xu, M.; Zhang, Z.; Wen, G.; Peng, F.; Yu, A.; Bai, Z.; Sun, Y.; Zhang, L.; Jiang, Z.; Chen, Z. Boron Nitride Membranes with a Distinct Nanoconfinement Effect for Efficient Ethylene/Ethane Separation. *Angew. Chem., Int. Ed.* **2019**, *131*, 14107−14113.

(13) Dou, H.; Xu, M.; Jiang, B.; Wen, G.; Zhao, L.; Wang, B.; Yu, A.; Bai, Z.; Sun, Y.; Zhang, L.; Chen, Z.; Jiang, Z. Bioinspired Graphene Oxide Membranes with Dual Transport Mechanisms for Precise Molecular Separation. *Adv. Funct. Mater.* **2019**, *29*, 1905229.

(14) Ying, W.; Peng, X. Graphene oxide nanoslit-confined AgBF$_4$/ionic liquid for efficiently separating olefin from paraffin. *Nanotechnology* **2019**, *31*, 085703.

(15) Kim, M.; Kang, S. W. PEBAX-1657/Ag nanoparticles/7,7,8,8-tetracyanoquinodimethane complex for highly permeable composite membranes with long-term stability. *Sci. Rep.* **2019**, *9*, 4266.

(16) Zarca, R.; Campos, A. C. C.; Ortiz, A.; Gorri, D.; Ortiz, I. Comprehensive study on PVDF-HFP/BMImBF$_4$/AgBF$_4$ membranes for propylene purification. *J. Membr. Sci.* **2019**, *572*, 255−261.

(17) Tomé, L. C.; Mecerreyes, D.; Freire, C. S. R.; Rebelo, L. P. N.; Marrucho, I. M. Polymeric ionic liquid membranes containing IL−Ag$^+$ for ethylene/ethane separation via olefin-facilitated transport. *J. Mater. Chem. A.* **2014**, *2*, 5631−5639.

(18) Jeong, S.; Sohn, H.; Kang, S. W. Highly permeable PEBAX-1657 membranes to have long-term stability for facilitated olefin transport. *Chem. Eng. J.* **2018**, *333*, 276−279.

(19) Dou, H.; Jiang, B.; Xiao, X.; Xu, M.; Tantai, X.; Wang, B.; Sun, Y.; Zhang, L. Novel protic ionic liquid composite membranes with fast and selective gas transport nanochannels for ethylene/ethane separation. *ACS Appl. Mater. Interfaces* **2018**, *10*, 13963−13974.

(20) Trivedi, T. J.; Lee, J. H.; Lee, H. J.; Jeong, Y. K.; Choi, J. W. Deep eutectic solvents as attractive media for CO$_2$ capture. *Green Chem.* **2016**, *18*, 2834−2842.

(21) Lin, H.; Gong, K.; Hykys, P.; Chen, D.; Ying, W.; Sofer, Z.; Yan, Y.; Li, Z.; Peng, X. Nanoconfined deep eutectic solvent in laminated MXene for efficient CO$_2$ separation. *Chem. Eng. J.* **2021**, *405*, 126961.

(22) Lian, S.; Li, R.; Zhang, Z.; Liu, Q.; Song, C.; Lu, S. Improved CO$_2$ separation performance and rinterfacial affinity of composite membranes by incorporating amino acid-based deep eutectic solvents. *Sep. Purif. Technol.* **2021**, *272*, 118953.

(23) Francisco, M.; van den Bruinhorst, A.; Kroon, M. C. Low-transition-temperature mixtures (LTTMs): a new generation of designer solvents. *Angew. Chem., Int. Ed.* **2013**, *52*, 3074−3085.

(24) Karimi, M. B.; Mohammadi, F.; Hooshyari, K. Potential use of deep eutectic solvents (DESs) to enhance anhydrous proton conductivity of Nafion 115 membrane for fuel cell applications. *J. Membr. Sci.* **2020**, *611*, 118217.

(25) Kuttiani Ali, J.; Maher Chabib, C.; Abi Jaoude, M.; Alhseinat, E.; Teotia, S.; Patole, S.; Hussain Anjum, D.; Qattan, I. Enhanced removal of aqueous phenol with polyimide ultrafiltration membranes embedded with deep eutectic solvent-coated nanosilica. *Chem. Eng. J.* **2021**, *408*, 128017.

(26) Xiong, D.; Zhang, Q.; Ma, W.; Wang, Y.; Wan, W.; Shi, Y.; Wang, J. Temperature-switchable deep eutectic solvents for selective separation of aromatic amino acids in water. *Sep. Purif. Technol.* **2021**, *265*, 118479.

(27) Hanada, T.; Goto, M. Synergistic deep eutectic solvents for lithium extraction. *ACS Sustainable Chem. Eng.* **2021**, *9*, 2152−2160.

(28) Macchioni, V.; Carbone, K.; Cataldo, A.; Fraschini, R.; Bellucci, S. Lactic acid-based deep natural eutectic solvents for the extraction of bioactive metabolites of Humulus lupulus L.: Supramolecular organization, phytochemical profiling and biological activity. *Sep. Purif. Technol.* **2021**, *264*, 118039.

(29) Schiavi, P. G.; Altimari, P.; Branchi, M.; Zanoni, R.; Simonetti, G.; Navarra, M. A.; Pagnanelli, F. Selective recovery of cobalt from mixed lithium ion battery wastes using deep eutectic solvent. *Chem. Eng. J.* **2021**, *417*, 129249.

(30) Shi, J.; Sun, T.; Bao, J.; Zheng, S.; Du, H.; Li, L.; Yuan, X.; Ma, T.; Tao, Z. Water-in-Deep Eutectic Solvent" Electrolytes for High-Performance Aqueous Zn-Ion Batteries. *Adv. Funct. Mater.* **2021**, *31*, 2102035.

(31) Deng, R.; Sun, Y.; Bi, H.; Dou, H.; Yang, H.; Wang, B.; Tao, W.; Jiang, B. Deep Eutectic Solvents As Tuning Media Dissolving Cu$^+$ Used in Facilitated Transport Supported Liquid Membrane for Ethylene/Ethane Separation. *Energy Fuels* **2017**, *31*, 11146−11155.

(32) Sun, Y.; Bi, H.; Dou, H.; Yang, H.; Huang, Z.; Wang, B.; Deng, R.; Zhang, L. A Novel Copper(I)-Based Supported Ionic Liquid Membrane with High Permeability for Ethylene/Ethane Separation. *Ind. Eng. Chem. Res.* **2017**, *56*, 741−749.

(33) Smith, E. L.; Abbott, A. P.; Ryder, K. S. Deep eutectic solvents (DESs) and their applications. *Chem. Rev.* **2014**, *114*, 11060−11082.

(34) Dou, H.; Xu, M.; Wang, B.; Zhang, Z.; Wen, G.; Peng, F.; Zarshenas, K.; Luo, D.; Yu, A.; Bai, Z.; Jiang, Z.; Chen, Z. Self-Assembled Facilitated Transport Membranes with Tunable Carrier Distribution for Ethylene/Ethane Separation. *Adv. Funct. Mater.* **2021**, *31*, 2104349.

(35) Jiang, B.; Zhou, J.; Xu, M.; Dou, H.; Zhang, H.; Yang, N.; Zhang, L. Multifunctional ternary deep eutectic solvent-based membranes for the cost-effective ethylene/ethane separation. *J. Membr. Sci.* **2020**, *610*, 118243.

(36) Xu, M.; Jiang, B.; Dou, H.; Yang, N.; Xiao, X.; Tantai, X.; Sun, Y.; Zhang, L. Double-salt ionic liquid derived facilitated transport membranes for ethylene/ethane separation. *J. Membr. Sci.* **2021**, *639*, 119773.

(37) Dou, H.; Xu, M.; Wang, B.; Zhang, Z.; Luo, D.; Shi, B.; Wen, G.; Mousavi, M.; Yu, A.; Bai, Z.; Jiang, Z.; Chen, Z. Analogous Mixed Matrix Membranes with Self-Assembled Interface Pathways. *Angew. Chem., Int. Ed.* **2021**, *60*, 5864−5870.

(38) Lee, Y.-Y.; Penley, D.; Klemm, A.; Dean, W.; Gurkan, B. Deep Eutectic Solvent Formed by Imidazolium Cyanopyrrolide and Ethylene Glycol for Reactive CO_2 Separations. *ACS Sustainable Chem. Eng.* **2021**, *9*, 1090−1098.

(39) Karimi, M. B.; Mohammadi, F.; Hooshyari, K. Effect of deep eutectic solvents hydrogen bond acceptor on the anhydrous proton conductivity of Nafion membrane for fuel cell applications. *J. Membr. Sci.* **2020**, *605*, 118116.

(40) Gu, Y.; Jérôme, F. Glycerol as a sustainable solvent for green chemistry. *Green Chem.* **2010**, *12*, 1127−1138.

(41) Yang, D.; Hou, M.; Ning, H.; Zhang, J.; Ma, J.; Yang, G.; Han, B. Efficient SO_2 absorption by renewable choline chloride−glycerol deep eutectic solvents. *Green Chem.* **2013**, *15*, 2261−2265.

(42) Behr, A.; Eilting, J.; Irawadi, K.; Leschinski, J.; Lindner, F. Improved utilisation of renewable resources: New important derivatives of glycerol. *Green Chem.* **2008**, *10*, 13−30.

(43) Matsuoka, A.; Kamio, E.; Mochida, T.; Matsuyama, H. Facilitated O_2 transport membrane containing Co (II)-salen complex-based ionic liquid as O_2 carrier. *J. Membr. Sci.* **2017**, *541*, 393−402.

(44) Dou, H.; Jiang, B.; Xiao, X.; Xu, M.; Wang, B.; Hao, L.; Sun, Y.; Zhang, L. Ultra-stable and cost-efficient protic ionic liquid based facilitated transport membranes for highly selective olefin/paraffin separation. *J. Membr. Sci.* **2018**, *557*, 76−86.

(45) Jiang, B.; Dou, H.; Wang, B.; Sun, Y.; Huang, Z.; Bi, H.; Zhang, L.; Yang, H. Silver-Based Deep Eutectic Solvents as Separation Media: Supported Liquid Membranes for Facilitated Olefin Transport. *ACS Sustainable Chem. Eng.* **2017**, *5*, 6873−6882.

(46) de Castro, A. M.; Prasavath, D.; Bevilaqua, J. V.; Portugal, C. A. M.; Neves, L. A.; Crespo, J. G. Role of water on deep eutectic solvents (DES) properties and gas transport performance in biocatalytic supported DES membranes. *Sep. Purif. Technol.* **2021**, *255*, 117763.

(47) Kasahara, S.; Kamio, E.; Ishigami, T.; Matsuyama, H. Effect of water in ionic liquids on CO2 permeability in amino acid ionic liquid-based facilitated transport membranes. *J. Membr. Sci.* **2012**, *415−416*, 168−175.

(48) Hong, S.; Kim, J. Y.; Kang, Y. S. Effect of water on the facilitated transport of olefins through solid polymer electrolyte membranes. *J. Membr. Sci.* **2001**, *181*, 289−293.

(49) Rungta, M.; Zhang, C.; Koros, W. J.; Xu, L. Membrane-based ethylene/ethane separation: The upper bound and beyond. *AIChE J.* **2013**, *59*, 3475−3489.

(50) Faiz, R.; Li, K. Olefin/paraffin separation using membrane based facilitated transport/chemical absorption techniques. *Chem. Eng. Sci.* **2012**, *73*, 261−284.

(51) Merkel, T. C.; Blanc, R.; Ciobanu, I.; Firat, B.; Suwarlim, A.; Zeid, J. Silver salt facilitated transport membranes for olefin/paraffin separations: Carrier instability and a novel regeneration method. *J. Membr. Sci.* **2013**, *447*, 177−189.

(52) Kim, J. H.; Min, B. R.; Lee, K. B.; Won, J.; Kang, Y. S. Coordination structure of various ligands in crosslinked PVA to silver ions for facilitated olefin transport. *Chem. Commun.* **2002**, *22*, 2732−2733.

(53) Pinnau, I.; Toy, L. G. Solid polymer electrolyte composite membranes for olefin/paraffin separation. *J. Membr. Sci.* **2001**, *184*, 39−48.

(54) Sunderrajan, S.; Freeman, B.; Hall, C.; Pinnau, I. Propane and propylene sorption in solid polymer electrolytes based on poly (ethylene oxide) and silver salts. *J. Membr. Sci.* **2001**, *182*, 1−12.

(55) Hong, S. U.; Jin, J. H.; Won, J.; Kang, Y. S. Polymer-Salt Complexes Containing Silver Ions and Their Application to Facilitated Olefin Transport Membranes. *Adv. Mater.* **2000**, *12*, 968−971.

(56) Dou, H.; Jiang, B.; Zhang, L.; Xu, M.; Sun, Y. Synergy of high permeability, selectivity and good stability properties of silver-decorated deep eutectic solvent based facilitated transport membranes for efficient ethylene/ethane separation. *J. Membr. Sci.* **2018**, *567*, 39−48.